NASA TECHNICAL NOTE

NASA TN D-3151

NASA TN D-3151

FATIGUE-CRACK PROPAGATION AND RESIDUAL STATIC STRENGTH OF PH 15-7 Mo (TH 1050) STAINLESS STEEL

by C. Michael Hudson

Langley Research Center
Langley Station, Hampton, Va.

NATIONAL AERONAUTICS AND SPACE ADMINISTRATION • WASHINGTON, D. C. • DECEMBER 1965

NASA TN D-3151

FATIGUE-CRACK PROPAGATION AND RESIDUAL STATIC STRENGTH OF PH 15-7 Mo (TH 1050) STAINLESS STEEL

By C. Michael Hudson

Langley Research Center
Langley Station, Hampton, Va.

NATIONAL AERONAUTICS AND SPACE ADMINISTRATION

For sale by the Clearinghouse for Federal Scientific and Technical Information
Springfield, Virginia 22151 – Price $2.00

FATIGUE-CRACK PROPAGATION AND RESIDUAL STATIC STRENGTH OF PH 15-7 Mo (TH 1050) STAINLESS STEEL*

By C. Michael Hudson
Langley Research Center

SUMMARY

Fatigue-crack propagation and residual static-strength data from tests on 2-inch (5.1-cm) wide sheet specimens made of PH 15-7 Mo (TH 1050) stainless steel are presented in this report. In addition, the capabilities of McEvily and Illg's crack-growth analysis and Kuhn and Figge's residual strength analysis to correlate the test data have been investigated. Kuhn and Figge's equation for calculating the stress concentration factors for cracks was used in both analyses. Analysis of the data showed that the crack growth and residual strength analyses satisfactorily correlated the majority of the test data.

INTRODUCTION

Fatigue cracks have been known to propagate during essentially the entire service life of aircraft structures. Consequently, the prediction of fatigue-crack propagation rates, and of the residual static strength of parts containing fatigue cracks, is of considerable interest to the aircraft designer. (In this paper residual static strength is defined as the maximum load required to fail a specimen containing a crack divided by the area remaining in the critical section prior to the application of load.) A method of quantitatively predicting fatigue-crack growth rates in aluminum alloys was developed in reference 1. It was shown that the rate of crack growth was an explicit function of the product of the stress-concentration factor for the crack and the net section stress. A method of calculating stress-concentration factors based on Neuber's analysis of stresses around sharp notches (ref. 2) was developed in the crack-growth analysis. A simple engineering method for predicting the strength of cracked aluminum parts under static loading was subsequently developed in reference 3. The method described therein for calculating stress-concentration factors was also based on the Neuber analysis and is similar in many respects to the method of calculating stress-concentration factors

*The information presented herein was offered as a thesis in partial fulfillment of the requirements for the degree of Master of Science in Engineering Mechanics, Virginia Polytechnic Institute, Blacksburg, Virginia, April 1965.

outlined in reference 1. In this report the method developed in reference 3, and subsequently modified in reference 4, was used to calculate stress-concentration factors for both analyses.

The purposes of this investigation were (a) to provide fatigue-crack propagation and residual static-strength data on PH 15-7 Mo (TH 1050) stainless steel, and (b) to determine the capability of the two aforementioned analyses to correlate the test data. Tests were conducted on 2-inch (5.1-cm) wide sheet specimens. The fatigue-crack propagation tests were conducted at ratios of minimum stress to maximum stress of 0 and -1 under maximum stresses varying from 12 to 100 ksi (83 to 689 MN/m^2).

The capability of the residual static-strength analysis to predict the effects of changing specimen widths and of buckling restraint in the vicinity of the crack on residual static strength is also briefly considered.

SYMBOLS

The units used for the physical quantities defined in this paper are given both in U.S. Customary Units and in the International System of Units, SI (ref. 5). Appendix A presents factors relating these two systems of units.

A_1, A_2, A_3	constants in the fatigue-crack rate expression
a	one-half of the total length of a central symmetrical crack, in. or cm
E	Young's modulus of elasticity, ksi or giganewtons/meter^2 (GN/m^2)
E_u	secant modulus pertaining to tensile ultimate stress, ksi or GN/m^2
e	elongation in 2-inch (5.1-cm) gage length, percent
f_1, f_2	rate determining functions
K_{TN}	stress-concentration factor for a central crack (corrected for size effect)
K_u	static notch-strength factor
K_w	finite width factor
N	number of cycles
R	ratio of minimum stress to maximum stress
r	rate of fatigue-crack propagation, in./cycle or cm/cycle
S_f	fatigue limit (stress at 10^7 cycles), ksi or meganewtons/meter^2 (MN/m^2)

S_{net}	load divided by the instantaneous net section area $[(w - 2a)t]$, ksi or MN/m^2
S_o	load divided by the initial net section area $[(w - x)t]$, ksi or MN/m^2
S_u	predicted net section failing stress when buckling is prevented, ksi or MN/m^2
S_u^*	predicted net section failing stress when buckling is not prevented, ksi MN/m^2
t	specimen thickness, in. or cm
w	specimen width, in. or cm
x	length of the crack-starter notch, in. or cm
ρ'	Neuber material parameter, in. or cm (residual static-strength analysis)
ρ''	Neuber material parameter, in. or cm (fatigue-crack growth analysis)
σ_u	ultimate tensile strength, ksi or MN/m^2
σ_y	yield strength (0.2-percent offset), ksi or MN/m^2

SPECIMENS AND TESTS

Specimens

All specimens were made from PH 15-7 Mo stainless steel heattreated to Condition TH 1050. Details of the heat treatment are listed in table I. Tensile properties obtained by using standard ASTM tensile specimens (ref. 6) and the nominal chemical composition of the material are also listed in table I. The configurations of the fatigue-crack propagation and residual static-strength specimens are shown in figure 1. Sheet specimens 18 inches (45.7 cm) long, 2 inches (5.1 cm) wide, and nominally 0.025 inch (0.64 mm) thick were tested. Each specimen contained a central notch at which the fatigue crack was initiated. The configuration of the unnotched specimens used to establish the fatigue limit of the material at $R = 0$ is also shown in figure 1. These specimens were $12\frac{5}{8}$ inches (32.1 cm) long, 2 inches (5.1 cm) wide, and nominally 0.025 inch (0.64 mm) thick. Each specimen was fabricated so that the longitudinal axis of the specimen was parallel to the grain of the sheet.

The surface area through which the crack was expected to propagate was polished with a slurry of fine carborundum powder and water to facilitate observation of the crack. A reference grid (ref. 7) was photographically printed on the polished surface to mark

intervals in the path of the crack. Metallographic examination and tensile tests conducted on specimens bearing the grid indicated that the grid had no detrimental effect on the material.

Machines

Three fatigue testing machines were used in this investigation; an inertia force compensation machine, a subresonant machine, and a combination hydraulic and subresonant machine. Loads were continuously monitored on these machines by measuring the output of a strain-gage bridge attached to a weighbar through which the load was transmitted to the specimens. The maximum error in loading was ±1 percent of the applied load.

Procedure

Axial-load fatigue-crack propagation tests were conducted at $R = 0$ and $R = -1$. Stresses (based on the initial net section) ranging from 12 to 100 ksi (83 to 689 MN/m^2) were applied to propagate the fatigue cracks. In most cases, two specimens were tested at each stress level. In both the crack-growth and fatigue-life tests, the loads were kept constant throughout each test.

In order to follow crack growth, fatigue cracks were observed through 30 power microscopes while illuminated by a stroboscopic light. The number of cycles required to propagate the crack to each grid line was recorded. The tests were terminated when the cracks reached predetermined crack lengths. These specimens were saved for the residual static-strength portion of the investigation.

In almost all of the tests (crack growth, fatigue life, and static strength) the specimens were clamped between lubricated guides similar to those described in reference 8 in order to prevent buckling and out-of-plane vibrations during testing. Light oil was used to lubricate the surfaces of the specimens and the guides. For the crack-growth tests, a 1/8-inch (3.18-mm) wide cutout was made across the width of one plate to allow visual observation of the region of crack growth.

Constant-amplitude axial-load fatigue tests were conducted on the unnotched specimens to establish the fatigue limits of the material at $R = 0$. The fatigue limit was first approximated by constructing an alternating against mean stress diagram from the data in reference 9. Tests were then conducted at stress levels near the approximate fatigue limit until the actual limit had been determined. Tests were terminated either at 10^7 cycles or at failure of the specimen, whichever occurred first. The fatigue limit at $R = -1$ was obtained directly from reference 9.

→ 5

The crack-propagation specimens were removed from the fatigue machines following the crack-growth tests, and the crack lengths were measured. Each specimen was then subjected to a uniaxial tension load at a rate of 30,000 lbf/min (2.2 kN/S) until failure occurred.

RESULTS

Fatigue-Crack Propagation

The fatigue-crack growth data were correlated by using the fatigue-crack growth analysis developed in reference 1. This analysis is outlined briefly in appendix B. The stress-concentration factors for cracks were computed by the equation developed in reference 4. (See appendix C.)

In the fatigue-crack propagation tests the fatigue cracks initiated at both ends of the central notch and propagated towards the edges of the specimen. The difference in the lengths of the two cracks (measured from the center line of the specimen) was seldom greater than 0.05 inch (1.27 mm). The fatigue-crack propagation data for the two cracks initiated in each test were plotted in one figure, and a mean curve was faired between the two sets of data. When two tests were conducted at the same stress level, the two mean curves were superposed and another mean curve was faired. All the comparisons of the fatigue-crack growth data presented in this paper were made from these final mean curves.

The mean number of cycles required to propagate the cracks from a half-length a of 0.10 inch (2.54 mm) to specified half crack lengths is shown in table II. The numbers of cycles are referenced from a half crack length of 0.10 inch (2.54 mm) because it was considered (ref. 1) that fatigue-crack growth is no longer influenced by the shape of the starter notch at that length. The fatigue-crack propagation data are also presented as semilog plots in figures 2 and 3.

Fatigue-crack propagation rates were determined graphically by taking the slopes of the half crack length against cycles curves (plotted on a linear scale) at various crack lengths. These rates are plotted against $K_{TN}S_{net}$ in figures 4 and 5 for $R = 0$ and $R = -1$, respectively. Examination of these figures shows that the rate of fatigue-crack propagation in PH 15-7 Mo (TH 1050) stainless steel at $R = 0$ and -1 is in general a single-valued function of $K_{TN}S_{net}$.

The values of $\sqrt{\rho''}$ used to calculate K_{TN} were determined by the method outlined in reference 1. An expression for the critical value of $K_{TN}S_{net}$ at which fatigue-crack growth cannot occur was derived from the boundary condition stating that crack growth could not occur at values of $K_{TN}S_{net}$ equal to or less than the unnotched fatigue

limit of the material. Thus

$$(K_{TN}S_{net})_{crit} = S_f \tag{1}$$

Appendix C presents an expression (eq. (C1)) for K_{TN}:

$$K_{TN} = 1 + 2\,K_w\sqrt{a/\rho''} \tag{2}$$

where ρ'' is used for ρ' as noted in appendix C. Substituting equation (2) for K_{TN}

$$\left(1 + 2\,K_w\sqrt{a/\rho''}\right)S_{net} = S_f \tag{3}$$

The fatigue limit for unnotched PH 15-7 Mo (TH 1050) specimens at $R = -1$ was reported in reference 9 to be 80 ksi (551 MN/m^2). The fatigue limit for unnotched specimens at $R = 0$ was determined experimentally in this investigation to be 120 ksi (826 MN/m^2). (See table III.) In order to obtain S_{net} and a (and, consequently, K_w) in equation (3), ancillary tests were conducted at $R = 0$ and -1. Small fatigue cracks were initiated in the specimens at the lowest stress levels at which cracks could be started at the central notch. The initiation stresses were kept as low as possible in order to keep the residual compressive stresses ahead of the crack tip to a minimum (ref. 10). Once the cracks were initiated and propagating, the stresses were systematically reduced by small increments until the fatigue cracks were no longer propagating. These data are shown in table II. It was then possible to solve equation (3) for $\sqrt{\rho''}$ at both stress ratios. The value of $\sqrt{\rho''}$ was found to be 0.048 $in^{1/2}$ and 0.096 $in^{1/2}$ (0.24 $mm^{1/2}$ and 0.48 $mm^{1/2}$), respectively, for $R = 0$ and $R = -1$.

As a matter of interest, K_{TN} was calculated by using, for $\sqrt{\rho''}$, the value of $\sqrt{\rho'}$ derived in the analysis of the residual static strength data (next section). The fatigue-crack growth data were correlated reasonably well by using this residual strength $\sqrt{\rho'}$ (figs. 6 and 7). However, the boundary condition stating that crack growth could not occur at values of $K_{TN}S_{net}$ less than the unnotched fatigue limit of the material is violated.

The values of $K_{TN}S_{net}$ shown in figures 4 to 7 are far in excess of the actual stresses possible since plastic deformation mitigates some of the stress in the material at the crack tip. However, the results indicate that the rate of fatigue-crack growth in PH 15-7 Mo (TH 1050) stainless steel at $R = 0$ and -1 is a function of the product of the stress-concentration factor and the net section stress.

Residual Static Strength

The method (ref. 3) used in the analysis of the residual static-strength data is briefly described in appendix C. The experimental results of the residual static-strength

tests are shown in table IV and in figure 8. In this figure the residual static strength is plotted against the ratio of the crack length 2a to the specimen width w. The open symbols represent specimens tested with guide plates. These guide plates served to restrain buckling of the specimen in the vicinity of the crack. This buckling introduces additional stresses at the tip of the crack which lower the strength of the sheet. The solid curve in figure 8 is the variation of residual static strength with 2a/w calculated by using the analysis for guided specimens. This curve was obtained for various crack lengths by dividing the ultimate tensile strength of the material by K_u. Appendix C (eq. (C2)) defines K_u as

$$K_u = 1 + (K_{TN} - 1)\frac{E}{E_u} \tag{4}$$

The ratio E_u/E was evaluated from the complete stress-strain curve shown in figure 9. Since no master curves of $\sqrt{\rho'}$ against ultimate tensile strength are available for the stainless steels as there are for the titanium and aluminum alloys, the value of $\sqrt{\rho'}$ used in determining K_u was obtained by trial-and-error fitting of the calculated curve to the test data. This calculated curve was adjusted to give a good average fit to the data.

The solid symbols indicate specimens tested without guides. The dashed curve is the calculated strength for the unguided specimens. The calculated strength for the unguided specimens was obtained by adjusting the curve for the guided specimens with the empirical buckling correction (eq. (C3) in appendix C).

$$S_u^* = S_u \left[1 - 0.001(2a/t)\right] \tag{5}$$

In this case, the predicted strengths were significantly higher than the strengths found in the laboratory experiments.

The residual static-strength tests were conducted at the crack lengths generated in the fatigue-crack growth portion of the investigation. The plastic deformation which occurs at the crack tip during the residual static-strength tests was expected to mask any fatigue-induced residual stresses which could affect residual strength. It was reported in reference 11 that varying the fatigue-stress amplitude had virtually no effect on the residual static strength of centrally cracked AM 350 (CRT) stainless-steel sheet specimens.

As a matter of interest the residual static-strength data from this investigation were compared with the data obtained from a similar investigation (ref. 12) in which 8-inch (20.3-cm) wide centrally cracked PH 15-7 Mo (TH 1050) specimens were tested. The reference data are shown as the square symbols in figure 10. As was expected, the 8-inch (20.3-cm) wide specimens exhibited lower residual static strength than did the

2-inch (5.1-cm) wide specimens. The curves fitted through the two sets of data were computed by using the analysis from reference 3. The different values of $\sqrt{\rho'}$ used in getting good average fits to the two sets of data indicated that the method did not accurately predict the width effect for this alloy. However, the $\sqrt{\rho'}$ derived in fitting the curve to the data for 8-inch (20.3-cm) wide specimens provides a conservative but reasonable approximation of the residual strength of the 2-inch (5.1-cm) wide specimens (dashed curve).

DISCUSSION

As individual analysis methods both the fatigue-crack propagation and residual-static strength analyses correlated the test data adequately. The analysis of the fatigue crack propagation data was particularly good at both $R = 0$ and -1. Thus, the crack growth analysis has now been extended to an entirely new material, stainless steel.

The different values of $\sqrt{\rho''}$ determined for the $R = 0$ and $R = -1$ crack-growth data may have resulted from different degrees of microplastic deformation of the material ahead of the crack tip. In the $R = 0$ tests, this material is plastically deformed by tension loading only. In the $R = -1$ tests, the material is likewise plastically deformed and stretched by the tension portion of the loading cycle. On the compression portion of the cycle this stretched material may then be subjected to compressive stresses exceeding its compressive yield strength which is known to be reduced by the Bauschinger effect. Thus, in the $R = -1$ tests, the material ahead of the crack tip is subjected to more cyclic plastic deformation per load cycle than similar material in the $R = 0$ tests. It was reported in reference 13 that the values of $\sqrt{\rho''}$ for 2024-T3 and 7075-T6 aluminum alloys were applicable at both $R = 0$ and -1. A possible explanation of the different values of $\sqrt{\rho''}$ is that a high strength stainless steel like PH 15-7 Mo (TH 1050) is substantially more susceptible to modification by cyclic plastic deformation than the aluminum alloys.

Scatter in the results of the ancillary tests used to determine $\sqrt{\rho''}$ is another possible explanation for the difference in the $\sqrt{\rho''}$ values at $R = 0$ and -1. Small changes in any of the parameters in equation (2) can effect large changes in the value of $\sqrt{\rho''}$. Perhaps the ancillary tests, although very carefully conducted, were simply not sensitive enough to determine the parameters accurately.

The effect of loading frequency was not originally considered to be a significant parameter in the crack propagation portion of this investigation, since it was found in reference 1 that no consistent frequency effects existed for the aluminum alloys. Analysis of the data for the PH 15-7 Mo (TH 1050) indeed indicates that the range of loading frequencies, 40 to 1800 cpm (1 to 30 Hz) had little effect on the correlation of the data.

It was found in reference 9, however, that loading frequency had a noticeable effect on the fatigue life of PH 15-7 Mo (TH 1050). This finding, combined with the crack-growth results of this investigation, indicates that the loading frequency may affect primarily the crack initiation stage of the fatigue phenomenon. The manner in which loading frequency might affect crack initiation alone is not currently understood.

The residual static strength analysis fitted the data for the guided specimens reasonably well. However, the predicted strength of the unguided specimens was considerably higher than that found by experiment. This poor prediction indicates that the buckling correction (eq. (5)), which was originally developed for the aluminum alloys, is not applicable to other materials. Additional research on specimens subjected to varying degrees of buckling constraint would be quite helpful in more accurately defining the nature of the buckling correction.

The difference between the $\sqrt{\rho'}$ values for the 2-inch and the 8-inch (5.1- and 20.3-cm) wide specimens was unexpected. Unique values correlated the data quite well for sheet aluminum specimen ranging in width from 2.25 to 35 inches (5.7 to 88.8 cm). There was very little difference between the stainless steel tested in this investigation and that tested in the investigation reported in reference 12. The specimen thicknesses were identical, and the variation in tensile properties was 4 percent or less. The Knoop microhardness of representative specimens tested in the two investigations was nearly equal. In addition, the grain size of the specimens was quite similar. It is possible, however, that some undetected difference in the test conditions was responsible for this difference in the values of $\sqrt{\rho'}$.

The large differences between $\sqrt{\rho'}$ and $\sqrt{\rho''}$ determined for the fatigue-crack growth and the residual static-strength analyses might be explained by the differences in the basic failure mechanisms. It was proposed in the fatigue-crack growth analysis (ref. 1) that the material in the plastic zone ahead of the crack tip is cyclically work-hardened to its local fracture strength (which is not quantitatively defined). The crack then advances through this work-hardened zone into a region of non-work-hardened material where its progress is arrested. Progressive strain hardening begins once more and the sequence is repeated over and over again as the fatigue crack propagates through the material. In the case of residual static strength, it was proposed that failure occurs when the stress at the crack tip reaches the ultimate tensile strength of the material. It is obvious from these two mechanisms that the material being failed by fatigue-crack growth may be considerably different from the material being failed in the residual static-strength case. In the former case, the material is assumed to be substantially work-hardened by the repeated loadings, whereas in the latter case the material is work-hardened only during the application of the quarter load cycle required to fail it. It might be argued that in the residual static-strength tests the material ahead of the crack tip is work-hardened since the crack in the specimens was produced by cyclic loading.

However, a small increment of slow crack growth was observed to occur in each test prior to unstable crack growth. Consequently, material at the crack tip immediately before catastrophic failure had not been subjected to a great deal of cyclic work-hardening. Therefore, it is not unreasonable to expect that different values of the Neuber parameter could occur in the analysis of the two sets of data.

CONCLUDING REMARKS

Axial-load fatigue-crack propagation and residual static-strength tests were conducted on 2-inch (5.1-cm) wide sheet specimens made of PH 15-7 Mo (TH 1050) stainless steel. Analysis of the data showed that the fatigue-crack growth analysis and the residual static-strength analysis correlated the test data reasonably. Correlation of the fatigue-crack growth data at both $R = 0$ and $R = -1$ was particularly good. This good correlation indicates that the crack-growth analysis may be used successfully on data from tests on material other than the aluminum alloys (for which the analysis was originally developed).

The residual static-strength analysis fitted the data for the guided specimens quite well also. However, the analysis predicted much higher strengths for the unguided specimens than were obtained in the laboratory tests. This erroneously high prediction indicates the buckling correction used is applicable only to the aluminum alloys (for which the correction was originally developed). In addition, there was a significant difference in the Neuber material parameters for the 2-inch (5.1-cm) wide specimens tested in this investigation, and for the 8-inch (20.3-cm) wide specimens tested in a previous investigation. This difference may have resulted from some undetected variation in the conditions under which the specimens of different widths were tested.

to p. 14

Significantly different values of $\sqrt{\rho'}$ and $\sqrt{\rho''}$ were determined for the fatigue-crack growth and the residual static-strength analyses. This difference may be attributed to the different amounts of work hardening which occur in the material being failed in the two cases. In the crack-propagation case, considerable cyclic work hardening occurs prior to failure. In the residual-strength case the material is work hardened only during the application of the quarter cycle required to fail it.

Langley Research Center,
National Aeronautics and Space Administration,
Langley Station, Hampton, Va., September 9, 1965.

→ 14

APPENDIX A

CONVERSION OF U.S. CUSTOMARY UNITS TO SI UNITS

The International System of Units (SI) was adopted by the Eleventh General Conference of Weights and Measures, Paris, October 1960, in Resolution No. 12 (ref. 5). Conversion factors for the units used herein are given in the following table:

To convert from U.S. Customary Units	Multiply by –	To obtain SI units
lbf	4.448222	newton (N)
in.	2.54×10^{-2}	meter (m)
ksi	6.894757	meganewton/meter^2 (MN/m^2)
^{o}F	5/9 (^{o}F + 459.67)	degrees Kelvin (^{o}K)
cpm	1.67×10^{-2}	hertz (Hz)

Prefixes and symbols to indicate multiples of units are as follows:

Multiple	Prefix	Symbol
10^{-3}	milli	m
10^{-2}	centi	c
10^{3}	kilo	k
10^{6}	mega	M
10^{9}	giga	G

APPENDIX B

FATIGUE-CRACK GROWTH ANALYSIS

The growth of fatigue cracks was assumed in reference 1 to occur in two phases; a work-hardening phase and a crack-advancement phase. It was proposed that the number of cycles required to complete a work-hardening phase was a function of the product of the instantaneous net section stress S_{net} and the stress concentration factor for the crack K_{TN}. The boundary condition was imposed that insufficient work hardening would occur at values of $K_{TN}S_{net}$ below the fatigue limit S_f of unnotched specimens to permit propagation of a crack. From these proposed conditions, the following functional relationship for the average rate of fatigue-crack propagation was developed:

$$\log_{10} r = f_1(K_{TN}S_{net}) + f_2(K_{TN}S_{net}, S_f) \tag{B1}$$

An expression which fitted the test data on 2024-T3 and 2075-T6 aluminum alloys tested at $R = 0$ and which satisfied the function and boundary conditions was

$$\log_{10} r = A_1 K_{TN} S_{net} - A_2 - A_3 \left(\frac{S_f}{K_{TN}S_{net} - S_f} \right) \tag{B2}$$

This equation was also found to correlate with the data from tests on 2024-T3 and 7075-T6 aluminum alloys tested at $R = -1$ (ref. 13). The constants in this expression can be evaluated only by fitting the expression to actual test data. However, once these constants are determined, equation (B2) can, in principle, be used to predict crack-growth rates at any other stress level or configuration for the material.

The equation used in this investigation for calculating the stress-concentration factors for cracks K_{TN} was developed in reference 4 and is presented in appendix C of this report.

APPENDIX C

RESIDUAL STATIC-STRENGTH ANALYSIS

In the residual static-strength analysis (ref. 3), failure was assumed to occur in a cracked specimen when the stress at the tip of the crack reached the ultimate tensile strength of the material. The crack tip stress was defined as the product of the net section stress and the stress-concentration factor for the crack K_{TN}. The equation for calculating K_{TN} was developed from Neuber's theory of pointed notches. This equation had the following form after modification in reference 4:

$$K_{TN} = 1 + 2K_W\sqrt{a/\rho'} \tag{C1}$$

where a is one-half the length of the crack, K_W is a finite width factor determined from photoelastic studies by Dixon (ref. 14), and $\sqrt{\rho'}$ is Neuber's empirically determined material parameter. This parameter will be denoted as $\sqrt{\rho''}$ for the fatigue-crack propagation case. A plot of K_W against $2a/w$ is given in figure 11.

The factor K_{TN} was then corrected for plasticity by the equation

$$K_u = 1 + (K_{TN} - 1)\frac{E_u}{E} \qquad (S_{net} < \sigma_y) \tag{C2}$$

where K_u is the static notch-strength factor, E_u is the secant modulus corresponding to the stress at ultimate load, and E is Young's modulus.

An empirical buckling correction was proposed in reference 3 to account for the out-of-plane buckling which occurs in the material surrounding the crack when the test specimens are made from thin sheet material. This correction was given by the equation

$$S_u^* = S_u\,[1 - 0.001(2a/t)] \tag{C3}$$

where S_u^* is the predicted net section failing stress when buckling is not prevented, and S_u is the net section failing stress when buckling is prevented. It was recommended, however, when possible, that restraining guides be used to prevent buckling since this correction factor was not well substantiated.

REFERENCES

1. McEvily, Arthur J., Jr.; and Illg, Walter: The Rate of Fatigue-Crack Propagation in Two Aluminum Alloys. NACA TN 4394, 1958.

2. Neuber, H.: Theory of Notched Stresses: Principles for Exact Stress Calculation. J. W. Edwards (Ann Arbor, Mich.), 1946.

3. Kuhn, Paul; and Figge, I. E.: Unified Notch-Strength Analysis for Wrought Aluminum Alloys. NASA TN D-1259, 1962.

4. Kuhn, Paul: Notch Effects on Fatigue and Static Strength. Current Aeronautical Fatigue Problems, J. Schijve, J. R. Heath-Smith, and E. R. Welbourne, eds., Pergamon Press, c.1965, pp. 299-264.

5. Mechtly, E. A.: The International System of Units – Physical Constants and Conversion Factors. NASA SP-7012, 1964.

6. Anon.: Tentative Methods of Tension Testing of Metallic Materials. ASTM Designation E 8-61 T. Pt. 3 of 1961 Book of ASTM Standards Including Tentatives. Am. Soc. Testing Mater., c.1961, pp. 165-181.

7. Hudson, C. Michael: Fatigue-Crack Propagation in Several Titanium and Stainless-Steel Alloys and One Superalloy. NASA TN D-2331, 1964.

8. Brueggeman, W. C.; and Mayer, M., Jr.: Guides for Preventing Buckling in Axial Fatigue Tests of Thin Sheet-Metal Specimens. NACA TN 931, 1944.

9. Illg, Walter; and Castle, Claude B.: Axial-Load Fatigue Properties of PH 15-7 Mo Stainless Steel in Condition TH 1050 at Ambient Temperature and 550° F. NASA TN D-2358, 1964.

10. Hudson, C. Michael; and Hardrath, Herbert F.: Effects of Changing Stress Amplitude on the Rate of Fatigue-Crack Propagation in Two Aluminum Alloys. NASA TN D-960, 1961.

11. Gideon, D. N.; Marschall, C. W.; Holden, F. C.; and Hyler, W. S.: Exploratory Studies of Mechanical Cycling Fatigue Behavior of Materials for the Supersonic Transport. NASA CR-28, 1964.

12. Figge, I. E.: Residual Static Strength of Several Titanium and Stainless-Steel Alloys and One Superalloy at -109° F, 70° F, and 550° F. NASA TN D-2045, 1963.

13. Illg, Walter; and McEvily, Arthur, J., Jr.: The Rate of Fatigue-Crack Propagation for Two Aluminum Alloys Under Completely Reversed Loading. NASA TN D-52, 1959.

Photo p 16.

→ 16

14. Dixon, J. R.: Stress Distribution Around a Central Crack in a Plate Loaded in Tension; Effect of Finite Width of Plate. J. Roy. Aeron. Soc., Mar. 1960, pp. 141-145.

TABLE I.- MATERIAL DESCRIPTION

a. Heat treatment for Condition TH 1050: Heat to 1400° F (1033° K) for 90 minutes, cool to 60° F (289° K) within 1 hour, hold 60° F (289° K) for 30 minutes, heat to 1050° F (839° K) for 90 minutes, air cool to room temperature.

b. Average tensile properties of the PH 15-7 Mo (TH 1050) tested:

σ_u		σ_y		E		e, percent	No. of tests
ksi	MN/m^2	ksi	MN/m^2	ksi	GN/m^2		
207.5	1430	203.5	1400	30.4×10^3	209	8.3	4

c. Nominal chemical composition of PH 15-7 Mo, percent:

C	Mn	P	S	Si	N	Cr	Mo	Al	Fe
0.09 max.	1.00 max.	0.04 max.	0.03 max.	1.00 max.	6.50 to 7.75	14.00 to 16.00	2.00 to 3.00	0.75 to 1.50	Balance

TABLE II.- FATIGUE-CRACK PROPAGATION DATA

S_o		Number of cycles required to propagate a crack from a half-length a of 0.10 inch (0.254 cm) to a half-length a of –											Number of tests
ksi	MN/m^2	0.15 in. (0.381 cm)	0.20 in. (0.508 cm)	0.25 in. (0.635 cm)	0.30 in. (0.762 cm)	0.35 in. (0.888 cm)	0.40 in. (1.016 cm)	0.45 in. (1.144 cm)	0.50 in. (1.270 cm)	0.55 in. (1.400 cm)	0.60 in. (1.524 cm)	0.65 in. (1.651 cm)	
R = 0													
100	689	1,920	2,774	3,210	3,498	3,688	3,840						2
80	551	3,350	5,530	6,880	7,640	8,140	8,330	8,700					2
60	414	6,500	10,490	12,980	14,750	16,160							2
40	276	18,500	30,600	39,500	46,500	51,600	55,900	59,000	62,000				2
20	138	285,000	383,000	440,000	483,000	515,000	535,000	550,000	565,000	575,000	583,000	590,000	2
6	41	Crack did not propagate at a half crack length of 0.225 in. (5.71 mm)											1
R = -1													
80	551	1,680	2,450	2,960	3,310	3,560	3,740	3,845	3,910				2
60	414	4,350	6,950	8,550	9,550	10,150	10,500	10,740	10,840				2
40	276	14,500	24,530	31,500	36,000	39,300	42,000	44,200					2
20	138	142,000	215,000	265,000	301,000	328,000	351,000	368,000	381,000	393,000			2
17	117	210,000	345,000	440,000	510,000	560,000	595,000	620,000	640,000	655,000	665,000		1
15	103	420,000	650,000	799,000	900,000	970,000	1,020,000	1,065,000	1,100,000	1,120,000	1,145,000	1,160,000	1
12	83	1,020,000	1,590,000	1,840,000	2,000,000	2,120,000	2,200,000	2,260,000	2,300,000	2,340,000	2,360,000	2,380,000	1
10	69	Crack did not propagate at a half crack length of 0.125 in. (3.17 mm)											1

TABLE III.- FATIGUE LIFE DATA FOR UNNOTCHED SPECIMENS. R = 0.

Max. stress		Fatigue life
ksi	MN/m^2	
125	860	223,000 cycles
125	860	438,000 cycles
122	840	268,000 cycles
121	833	Did not fail in 14,705,000 cycles
120	826	Did not fail in 12,801,000 cycles
120	826	Did not fail in 12,231,000 cycles

TABLE IV.- RESIDUAL STATIC-STRENGTH RESULTS

2a/w	S_{net}		S_o at which fatigue crack propagated		R
	ksi	MN/m^2	ksi	MN/m^2	
0.250	189.8	1308	100	689	0
.275	190.6	1310	60	414	0
.305	189.0	1303	60	414	0
.430	[a]158.7	1094	100	689	0
.440	180.2	1242	40	276	-1
.470	181.2	1250	60	414	-1
.480	175.1	1209	80	551	0
.550	171.6	1182	40	276	-1
.615	[a]134.4	925	40	276	0
.715	149.2	1030	17	117	-1
.740	179.5	1238	20	138	-1
.765	[a]126.4	864	20	138	-1
.785	171.0	1179	20	138	0

[a]Tested without guide plates.

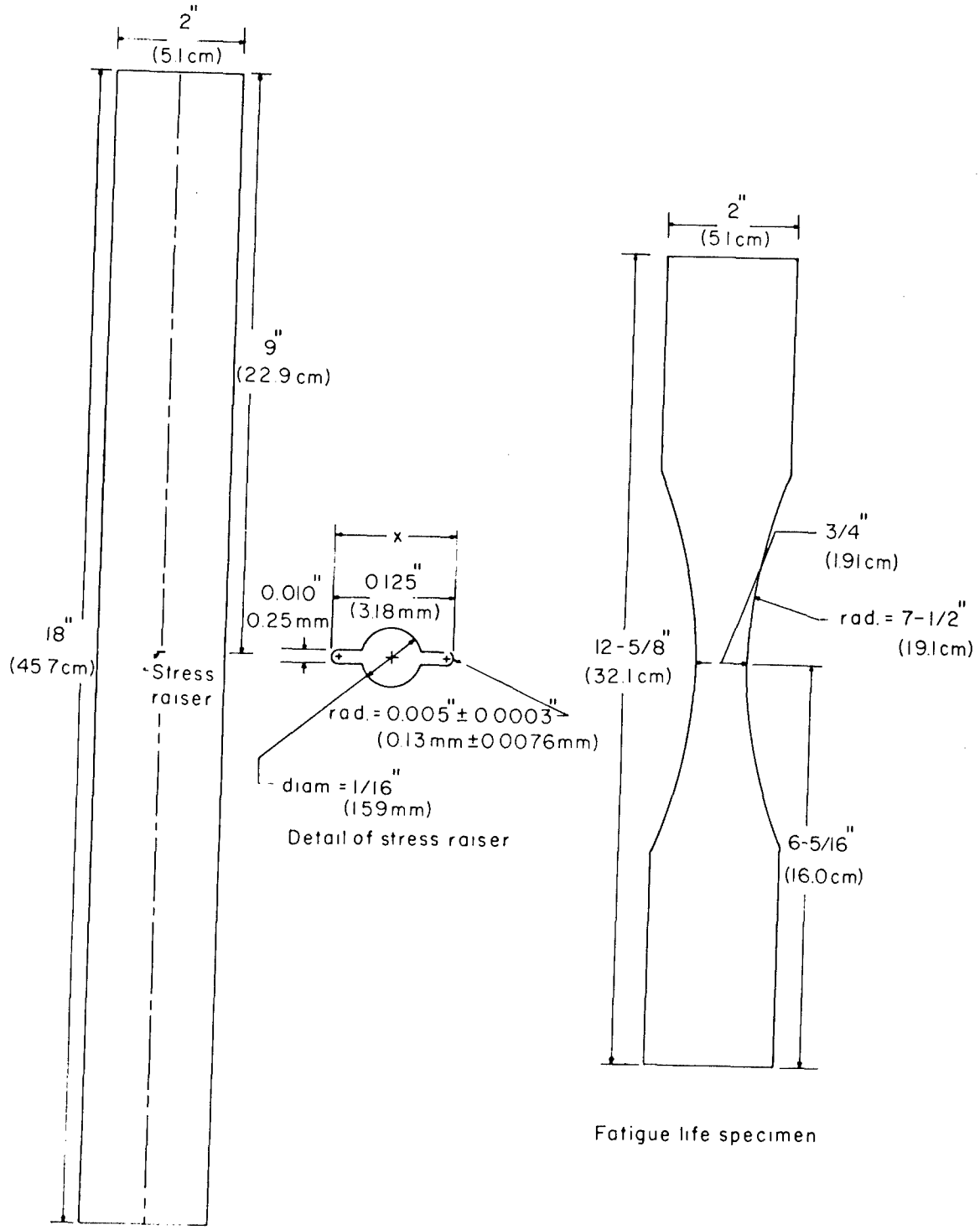

Figure 1.- Crack propagation and unnotched fatigue life specimen configurations. Specimen thickness, 0.025 in. (0.64 mm).

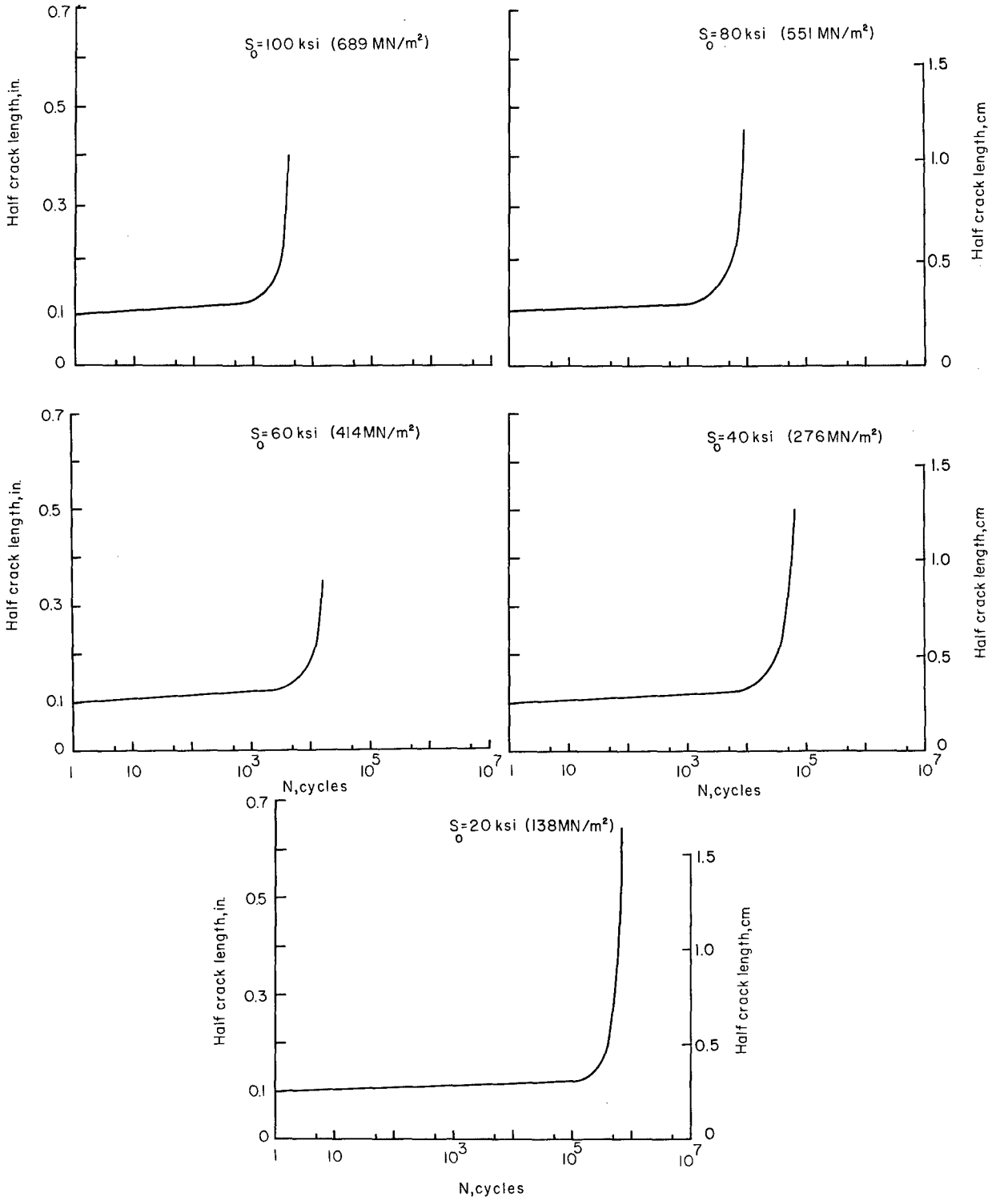

Figure 2.- Fatigue-crack propagation curves for PH 15-7 Mo (TH 1050) at R = 0.

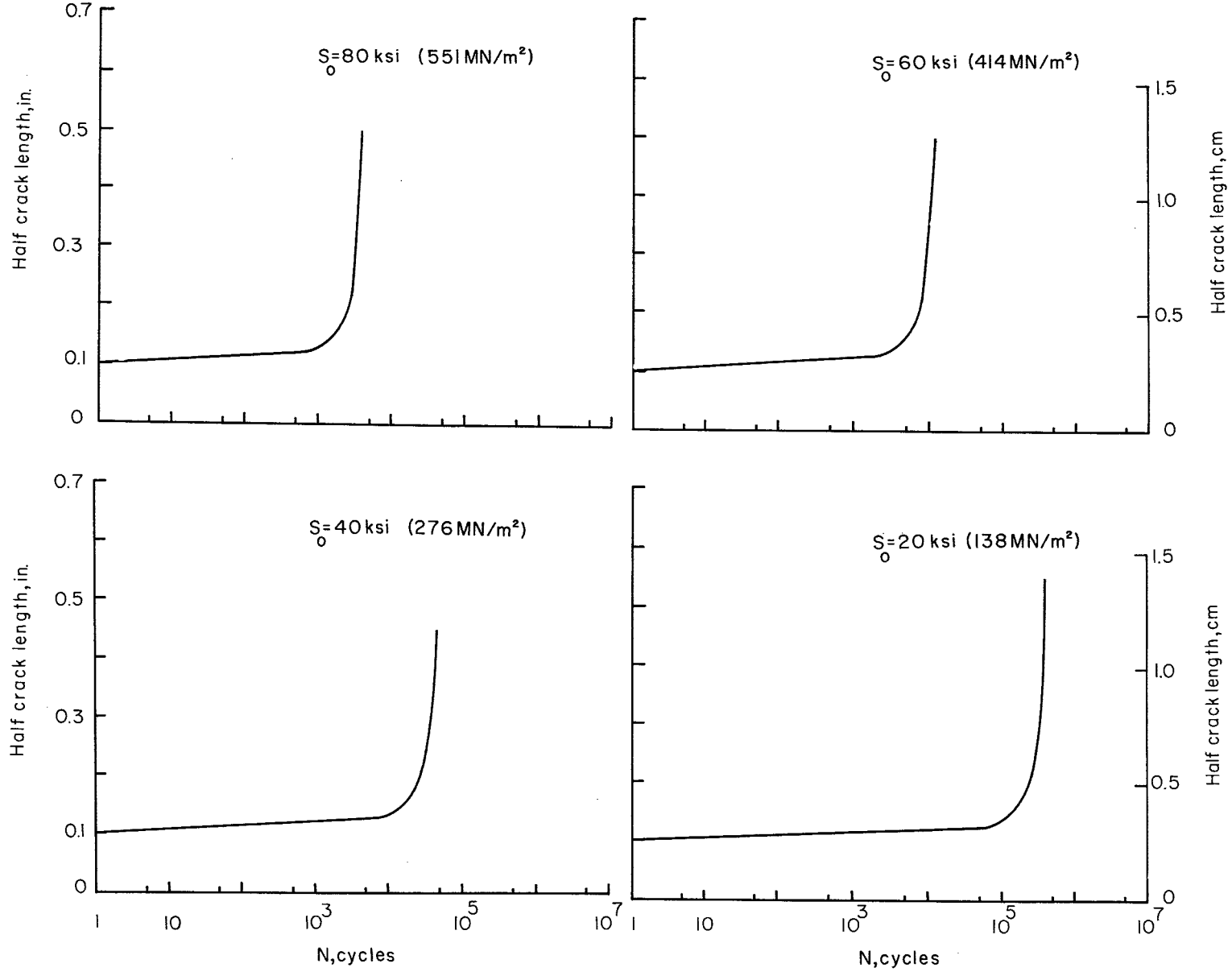

Figure 3.- Fatigue-crack propagation curves for PH 15-7 Mo (TH 1050) at R = -1.

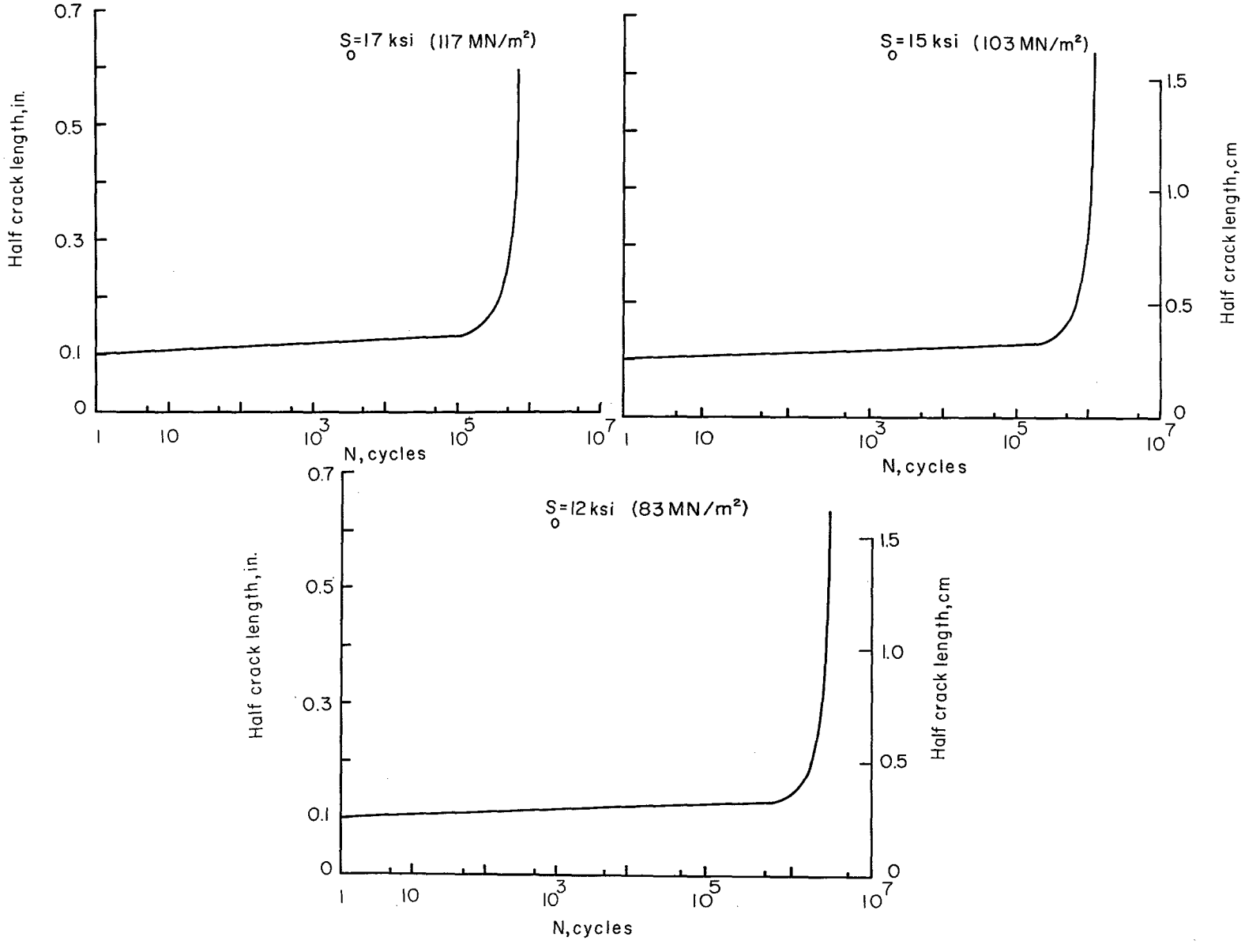

Figure 3.- Concluded.

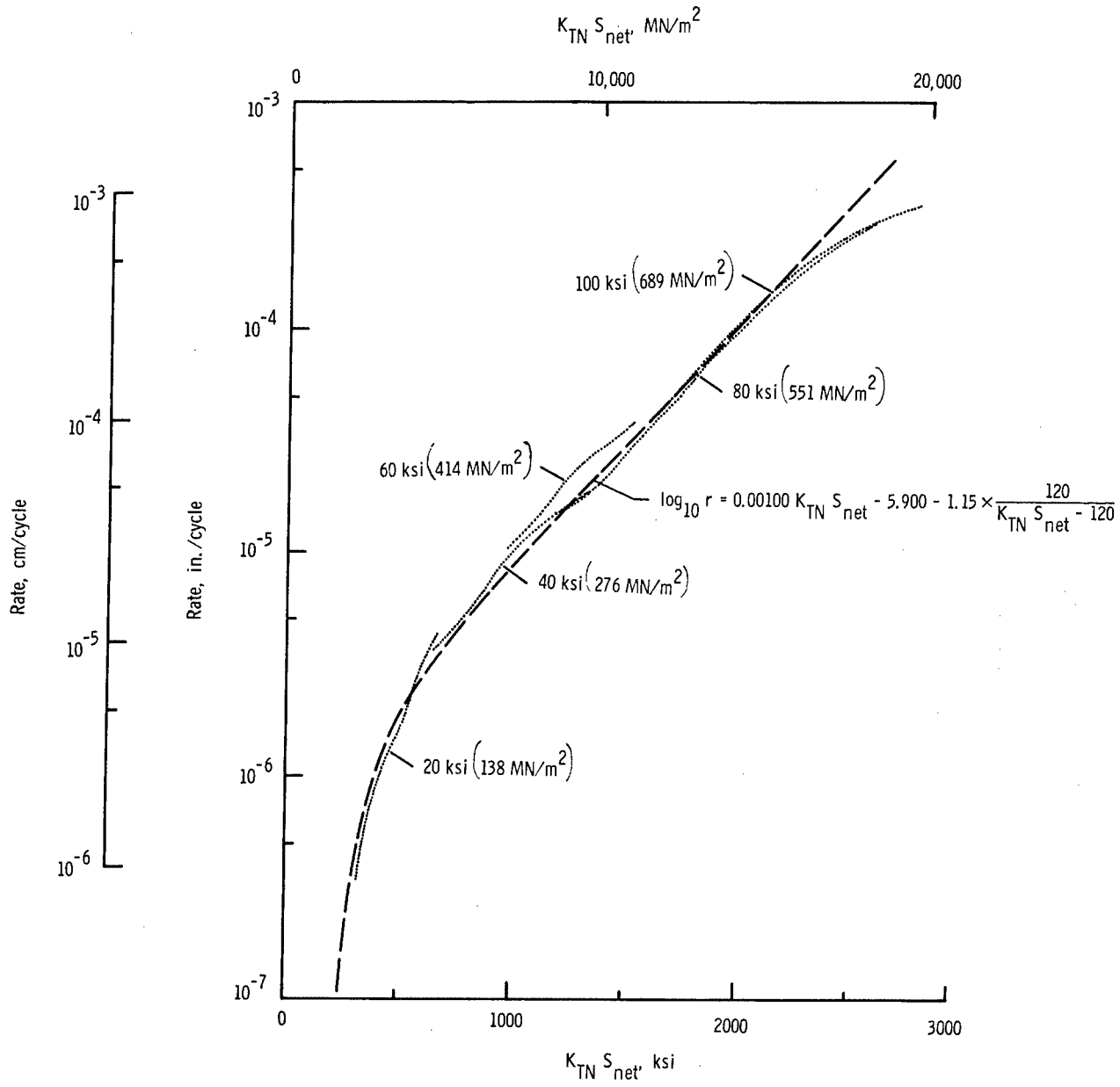

Figure 4.- Variation of rate of fatigue-crack growth with $K_{TN}S_{net}$ at R = 0. $\sqrt{\rho''}$ = 0.048 $in^{1/2}$ (0.24 $mm^{1/2}$).

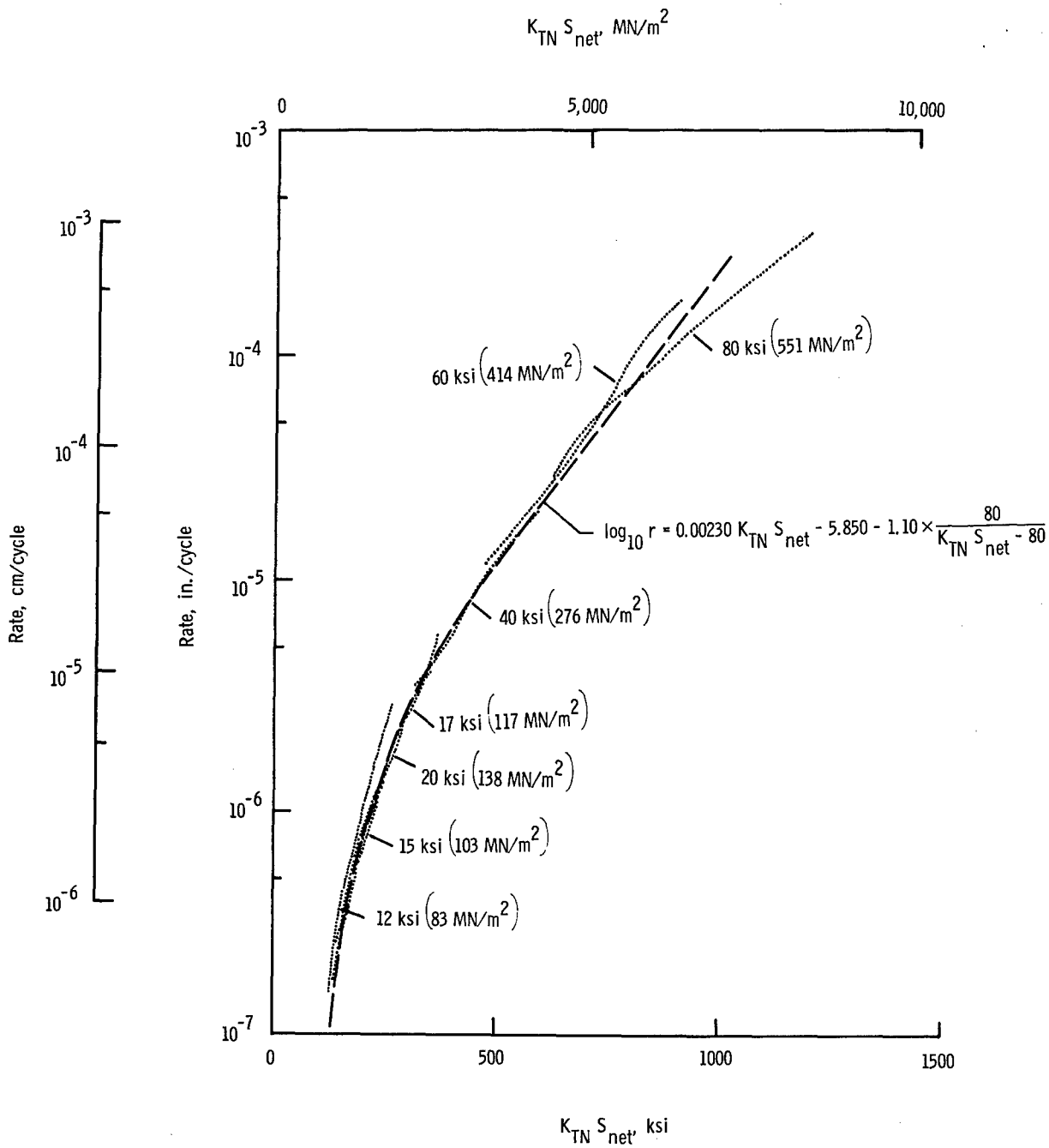

Figure 5.- Variation of rate of fatigue-crack growth with $K_{TN}S_{net}$ at R = -1. $\sqrt{\rho''}$ = 0.096 $in^{1/2}$ (0.48 $mm^{1/2}$).

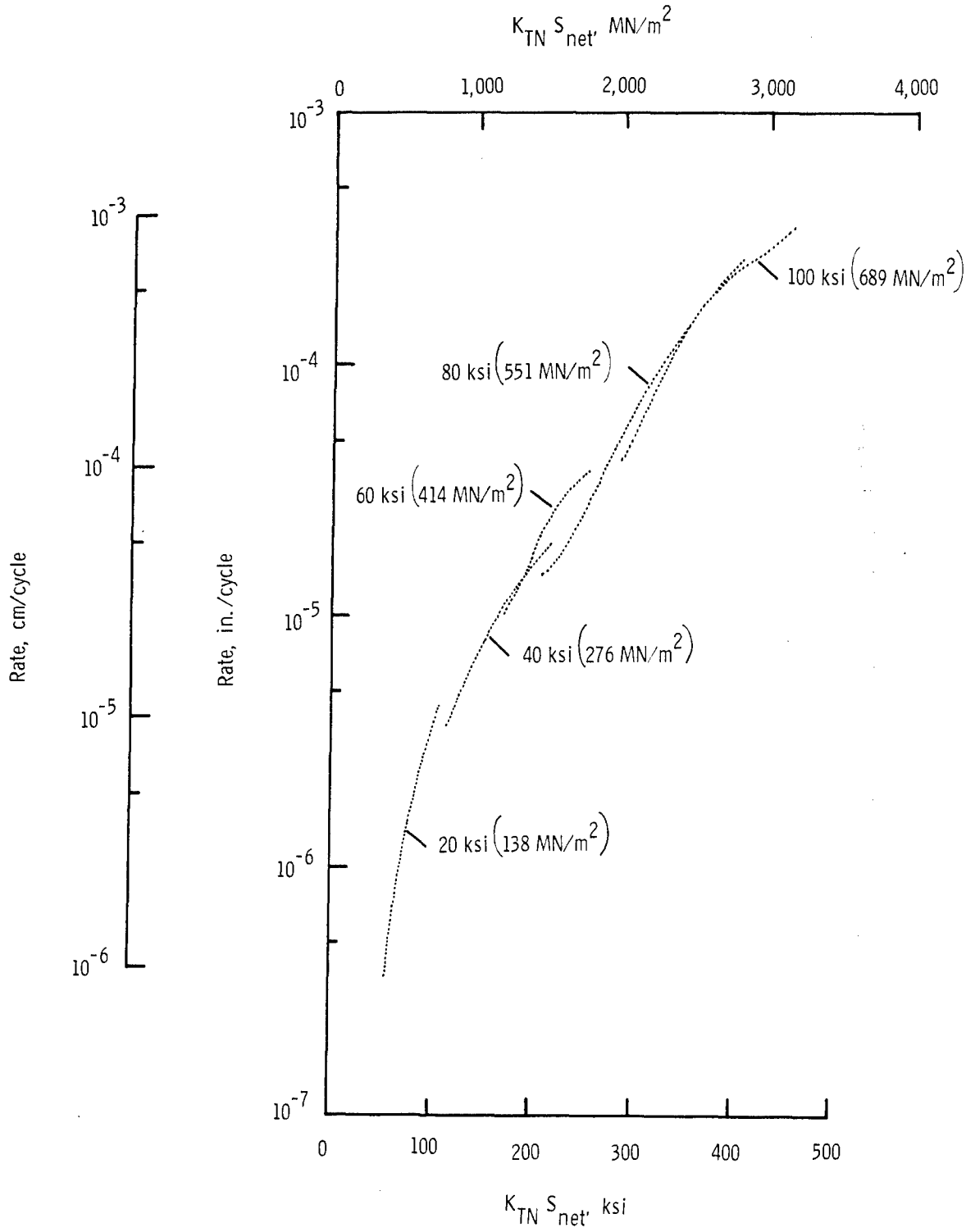

Figure 6.- Variation of rate of fatigue-crack growth with $K_{TN}S_{net}$ at R = 0. $\sqrt{\rho''}$ assumed 0.420 $in^{1/2}$ (0.67 $cm^{1/2}$).

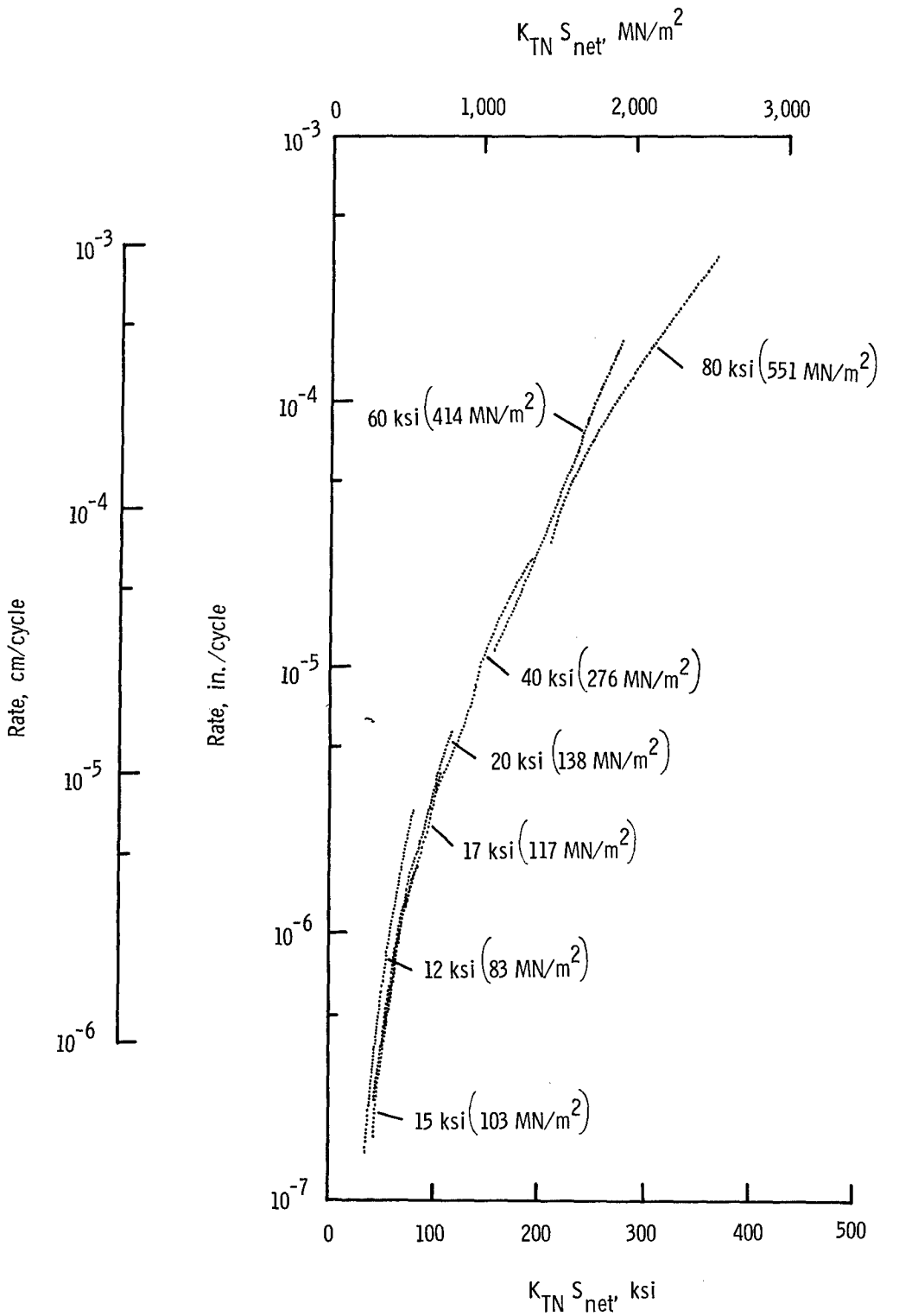

Figure 7.- Variation of rate of fatigue-crack growth with $K_{TN}S_{net}$ at R = -1. $\sqrt{\rho^*}$ assumed 0.420 $in^{1/2}$ (0.67 $cm^{1/2}$).

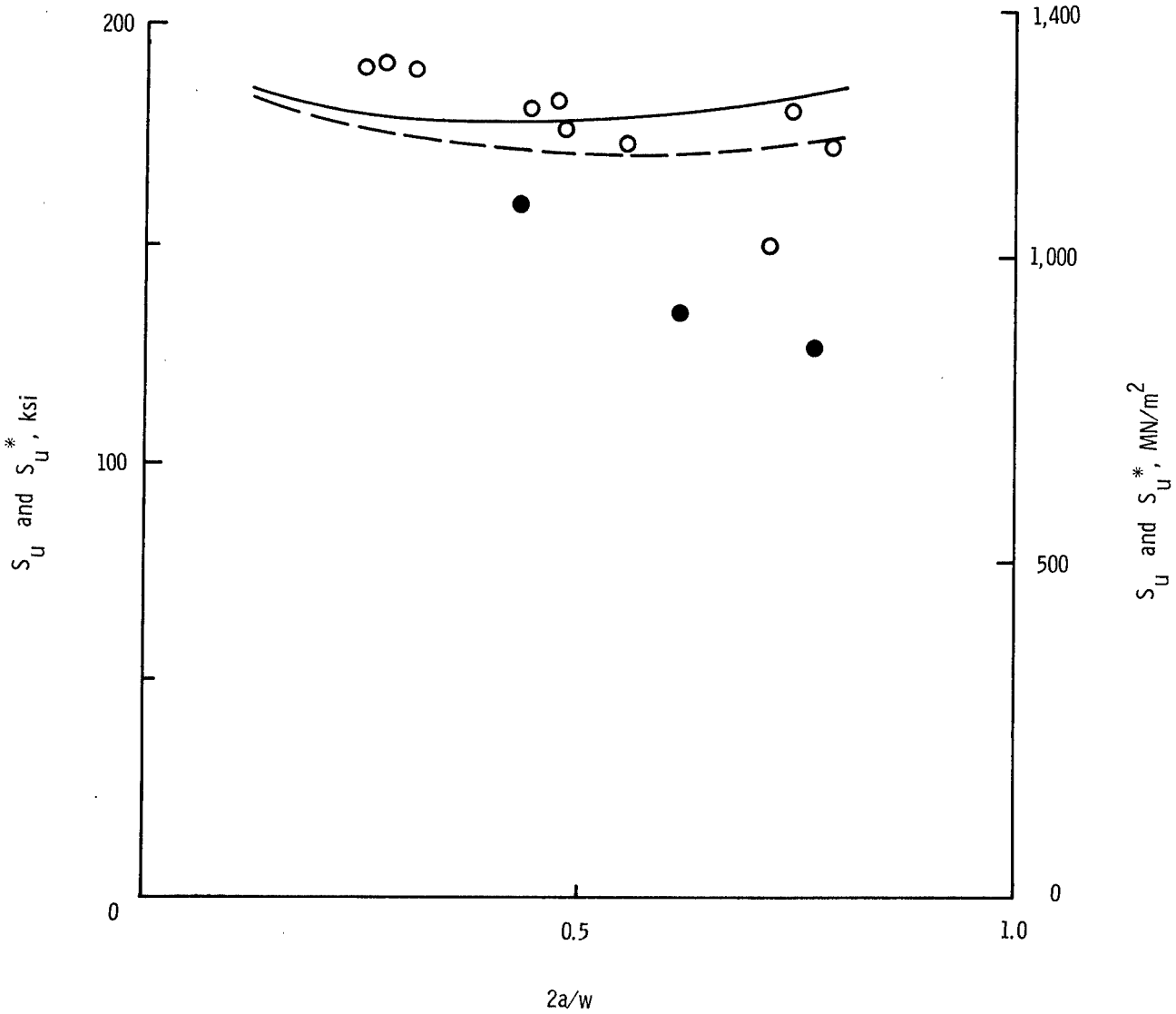

Figure 8.- Variation of the residual static strength of 2-inch (5.1-cm) wide PH 15-7 Mo (TH 1050) specimens with 2a/w. Calculated curves were fitted by using K_{TN}. Solid symbols indicate unguided specimens. $\sqrt{\rho'} = 0.420\ \text{in}^{1/2}\ (0.67\ \text{cm}^{1/2})$.

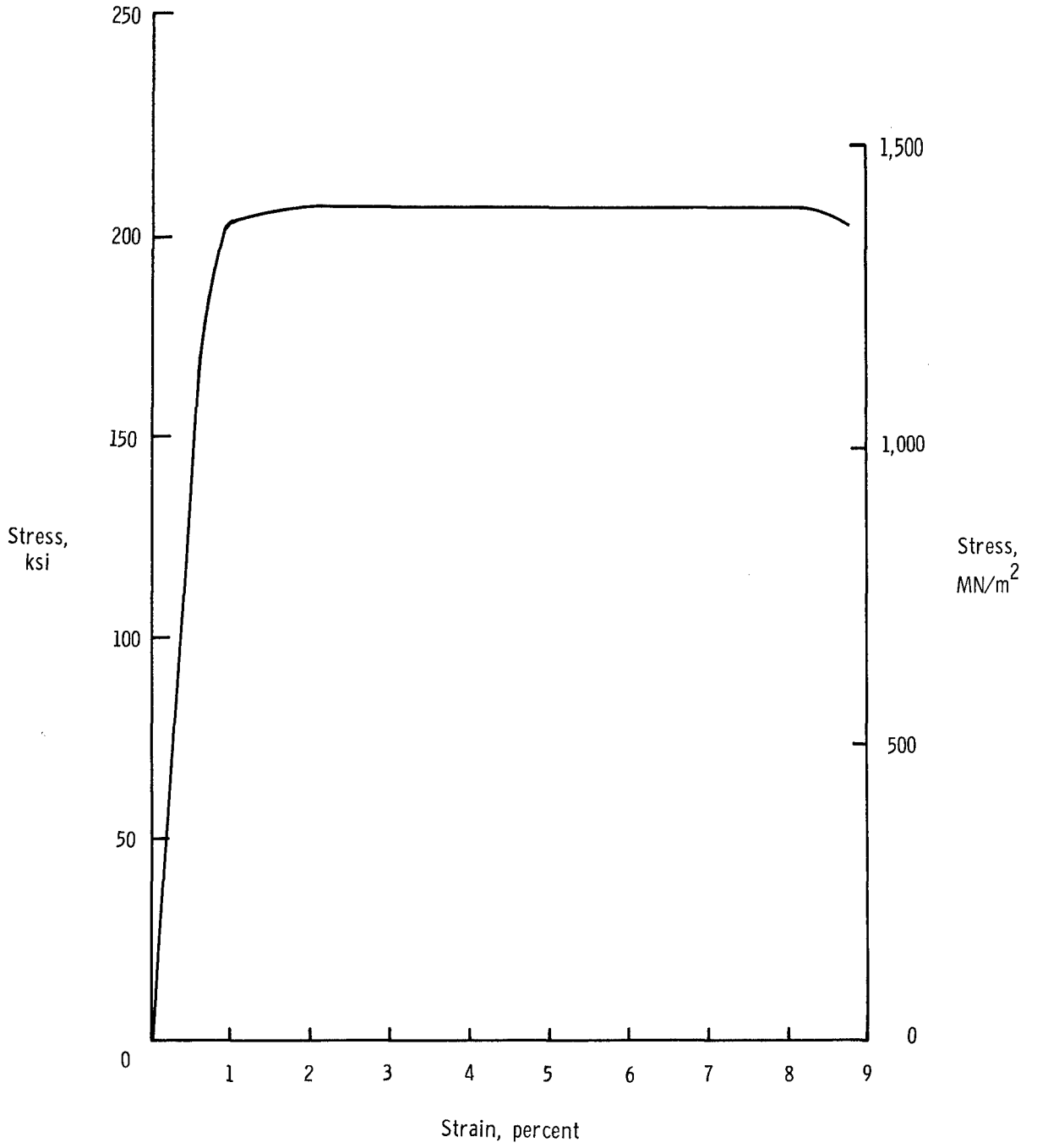

Figure 9.- Complete stress-strain curve for PH 15-7 Mo (TH 1050) stainless steel.

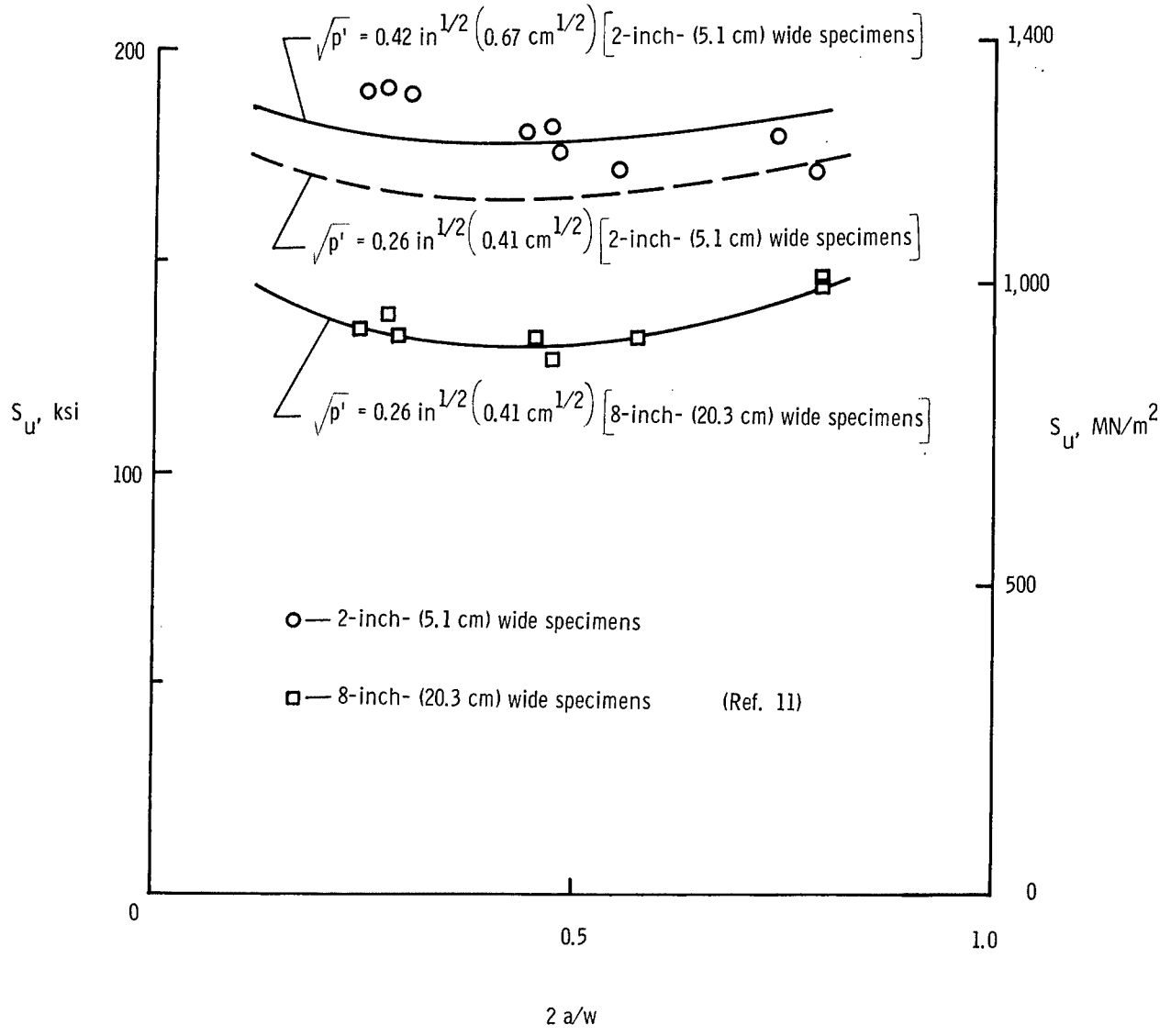

Figure 10.- Variation of the residual static strength of 2-inch and 8-inch (5.1-cm and 20.3-cm) wide PH 15-7 Mo (TH 1050) specimens with 2a/w. Calculated curves were fitted by using K_{TN}. All data points are for guided specimens.

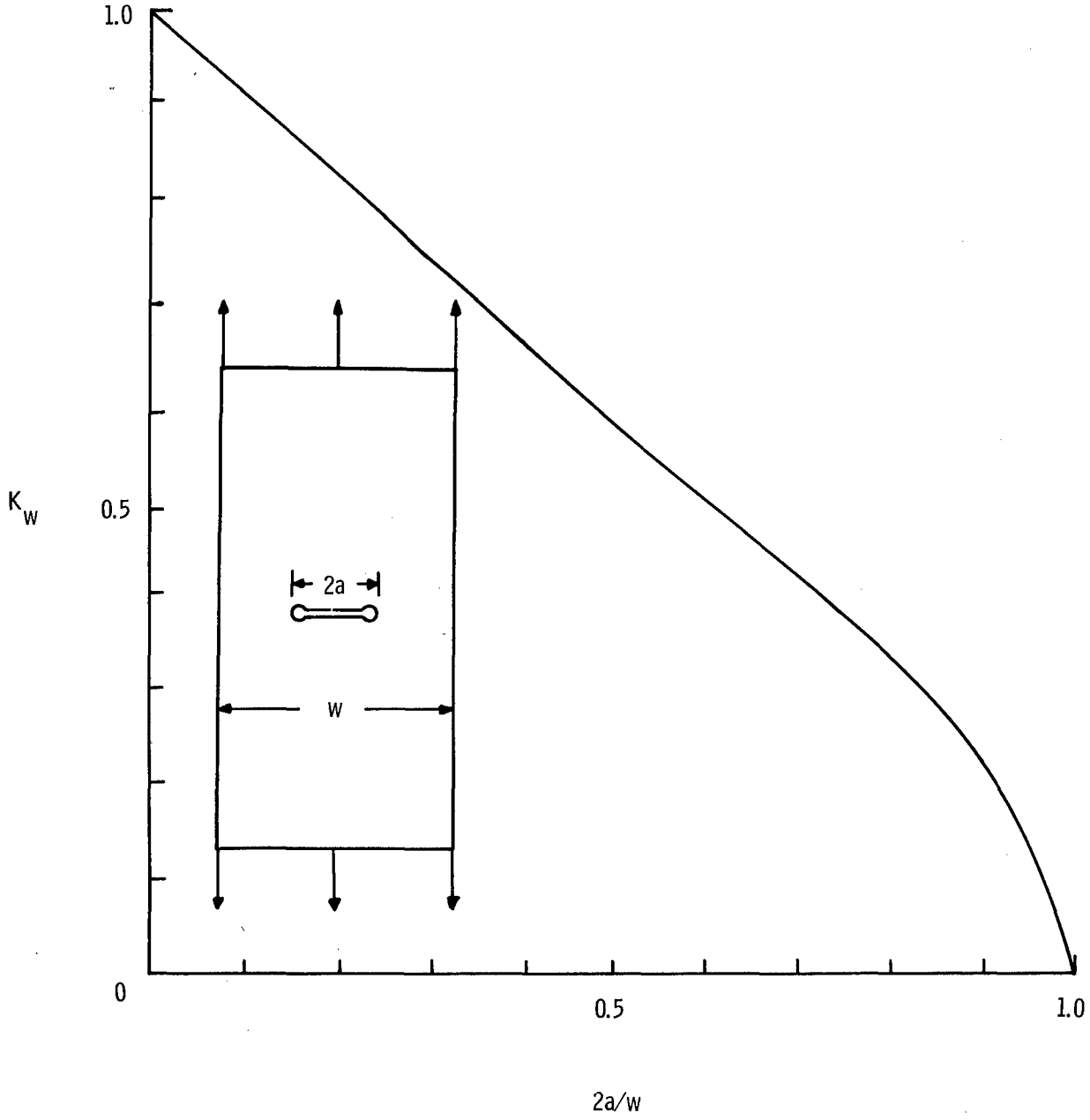

Figure 11.- Dixon's finite width correction.